

NLC Extraction Line Studies*

Y. M. Nosochkov and T. O. Raubenheimer
Stanford Linear Accelerator Center, Stanford University, Stanford, CA 94309

Abstract

In this note, we briefly review the current lattice of the NLC extraction line which was designed for the nominal NLC beam parameters [1, 2]. Then we describe the beam parameters for the high luminosity option with larger beam disruption parameter [3] and discuss its effect on beam loss in the extraction line. Finally, we present a summary of the optics study aimed at minimizing the beam loss with high disruption beams.

*Work supported by Department of Energy contract DE-AC03-76SF00515.

1 Introduction

In a linear collider, the rate of colliding bunches tends to be low when compared with a colliding beam storage ring. Fortunately, because the beams are not stored, the disruptive effect of the beam-beam forces is not a dynamical limitation and thus the beams can be focused to very small spot sizes to attain the high charge densities necessary to achieve the desired luminosity. When the high energy electron and positron beams collide, the space charge forces of the opposing beam cause large deflections. This has two effects: first, the effective beam emittance of the outgoing beam is increased due to the non-linearity of the beam-beam force and, second, when the high energy particles are deflected, they can radiate a significant fraction of their energies as synchrotron radiation which is referred to as beamstrahlung.

The NLC extraction line must be designed to transport this disrupted particle beam and the beamstrahlung photons away from the interaction point (IP) to dumps. In addition, the extraction line should provide diagnostics to fully instrument the collisions. This includes the ability to measure the outgoing beam angle and position, measure the energy spectrum of the outgoing beam, and measure the polarization of the outgoing beam. Because of the increased angular divergence and energy spread of the disrupted beam, it is a very difficult task to capture this beam and control it sufficiently well to make measurements of its properties.

In the next sections, we will review the present NLC design for the extraction line and some of the studies that have been made to further improve the performance. Many details of the present design are described in Ref. [4].

2 Current Lattice Design

The current lattice of the NLC extraction line is shown in Fig. 1. The magnet apertures are designed to allow the outgoing main beam and beamstrahlung photons to be transported to one shared dump at about 150 m from IP. The design provides 6 m of free space after IP to avoid interference with the quadrupoles needed to focus the incoming beam.

The optics consists of two multi-quad systems in the beginning and at the end of the beam-line, and a four-bend horizontal chicane in the middle. The first set of quadrupoles focuses the beam to a waist at the center of the horizontal chicane and then the second set of quadrupoles creates a parallel beam at the dump. The chicane creates 2 cm of horizontal dispersion at the secondary IP which will facilitate the measurement of the disrupted beam energy spread from which one can infer the luminosity spectrum. In addition, the chicane separates the particle beam from the core of the beamstrahlung photons which will allow measurements of the photon distribution. Finally, the electron beam waist and chicane provide an ideal location to measure the beam polarization using a Compton laser polarimeter, similar to the one developed for the SLC [5].

One of the main issues for the extraction line design is the minimization of beam loss; this is necessary to control backgrounds in the detector as well as the instrumentation in the extraction line. Most of the losses occur for the very low energy particles which experience large deflections in the magnets. For the typical NLC beam parameters [1, 2], the beam-

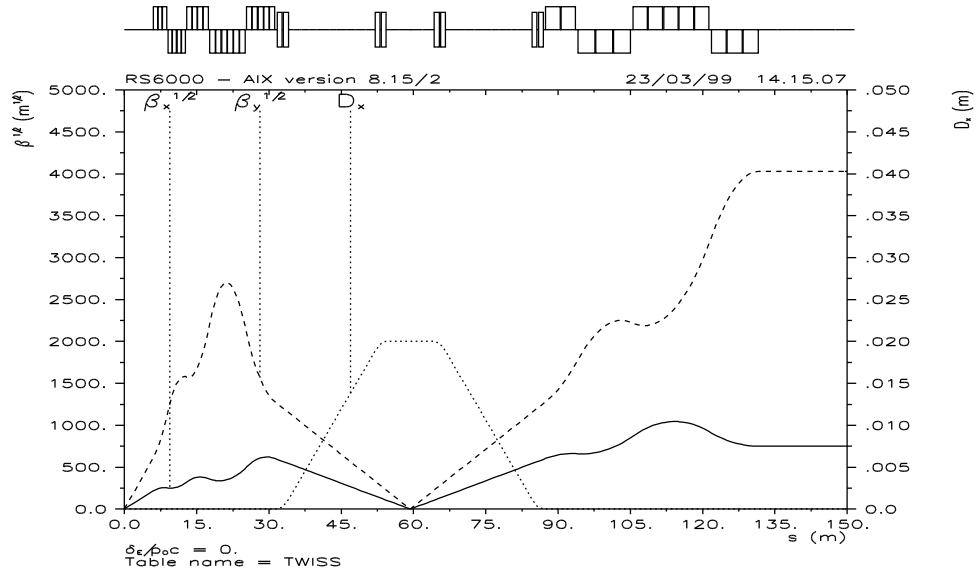


Figure 1: Current lattice of the NLC extraction line (IP at $s = 0$).

beam collisions generate an extremely broad energy spread in the outgoing beams. The spectrum at 500 GeV in the center-of-mass (cms) is narrower, but, with collisions at 1 TeV cms, the spectrum is so wide that there is still a significant number of electrons with energy deviations $\delta = \frac{\Delta p}{p}$ below -80% [6]. An example of the disrupted beam energy distribution is shown in Fig. 2 which corresponds to the beam parameters with the largest disruption at an energy of 1 TeV cms in the nominal NLC operation; these beam parameters are listed in Table 1 and are referred to as the ‘NLC 1 TeV case A’ parameter set. In this paper, we will refer to this case as the ‘nominal disruption’ case.

The low energy over-focusing in the extraction line is minimized with the use of alternating gradient multiple quadrupole systems rather than simple doublets. The strength of

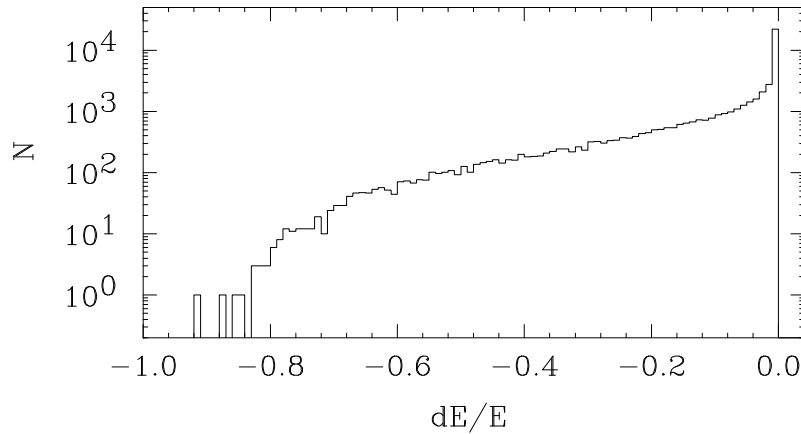


Figure 2: Energy distribution for the nominal disruption beam (NLC 1 TeV case A; 50,000 particles).

Table 1: IP parameters for the nominal disruption beam (NLC 1 TeV case A).

Beam parameter	Undisrupted	Disrupted
	x/y	x/y
Emittance (m·rad) [10^{-13}]	39/0.59	120/1.02
rms beam size (nm)	198/2.7	198/3.2
rms divergence (μ rad)	20/22	125/33
β^* (mm)	10/0.125	3.259/0.103
α^*	0/0	1.805/0.306
Energy cms (GeV)	1046	
Particles per bunch	$0.75 \cdot 10^{10}$	
Bunches per train	95	
Repetition rate (Hz)	120	
Disruption parameter	0.094/6.9	
Average energy loss per particle	9.5%	

individual quadrupoles in these systems is reduced compared to the doublet. This results in less over-focusing, smaller amplitude of the low energy particle oscillations and reduced beam loss.

For the beam parameters in Table 1 and optimized quadrupole strengths, the beam power losses in the extraction line are below 0.3 kW/m (see Fig. 3) with the total loss of 4.8 kW or 0.25% particles; the energy distribution of the lost and survived particles is shown in Fig. 4. It should be noted that at a cms energy of 500 GeV, the losses are roughly an order-of-magnitude smaller.

The azimuth distribution of particle loss is shown in Fig. 5, where $\theta = \text{atan}_x^y$ and x, y are the final coordinates of the lost particles. Due to somewhat larger horizontal beam size in the first half of the extraction line, there are more losses in the x -plane ($\theta = 0, \pm 180^\circ$)

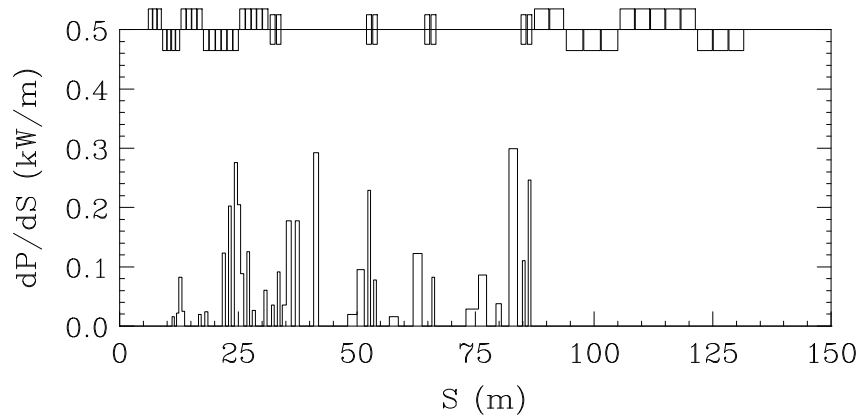


Figure 3: Power loss distribution for the nominal disruption beam in the current lattice (NLC 1 TeV case A).

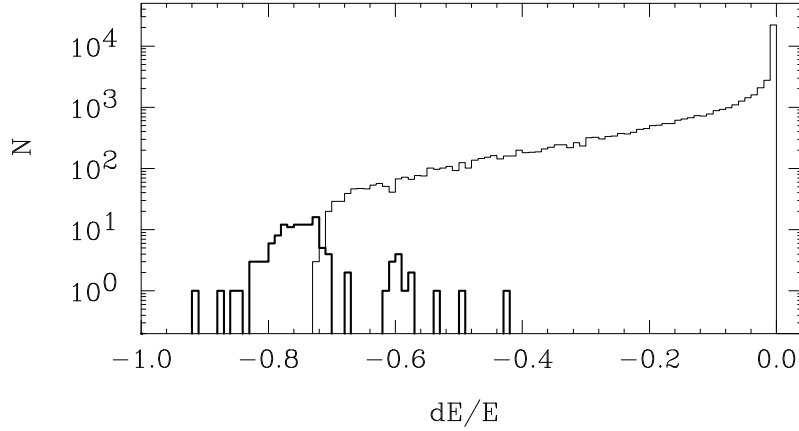


Figure 4: Energy distribution for the lost (thick line) and survived (thin) nominal disruption beam particles in the current lattice (NLC 1 TeV case A; 50,000 particles).

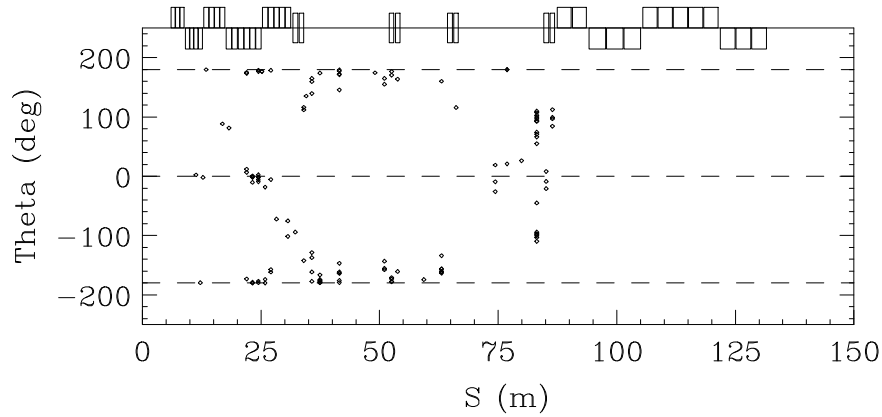


Figure 5: Azimuth distribution of lost particles (dots) for the nominal disruption beam (NLC 1 TeV case A).

than in the y -plane ($\theta = \pm 90^\circ$). Though not yet fully studied, it is hoped that this level of beam loss can be safely absorbed without significant complications.

3 High Disruption Beam

It has been reported recently that the NLC luminosity can be increased several times by using near-equal horizontal and vertical beta functions at the IP [3]. In this scenario, the undisrupted horizontal beam size at the IP is reduced and the vertical size is increased. The latter has an additional advantage of much looser tolerances in the final focus system. The disadvantage of this scenario is a significant increase in the angular beam divergence and beam energy spread after the collision. The IP parameters for the ‘high disruption’ case, similar to the case in Table 1, are listed in Table 2 [3]. The corresponding energy distribution for the disrupted beam is shown in Fig. 6.

Tables 1 and 2 show that the angular divergence of the high disruption beam is increased

Table 2: IP parameters for the ‘round(er) beam’ collisions at 1 TeV.

Beam parameter	Undisrupted	Disrupted
	x/y	x/y
Emittance (m·rad) [10^{-13}]	39/0.59	235/7.4
rms beam size (nm)	62.5/7.7	67.3/10.7
rms divergence (μ rad)	62.5/7.7	531/103
β^* (mm)	1.0/1.0	0.192/0.154
α^*	0/0	1.143/1.100
Energy cms (GeV)	1046	
Particles per bunch	$0.75 \cdot 10^{10}$	
Bunches per train	95	
Repetition rate (Hz)	120	
Disruption parameter	0.85/6.9	
Average energy loss per particle	41%	

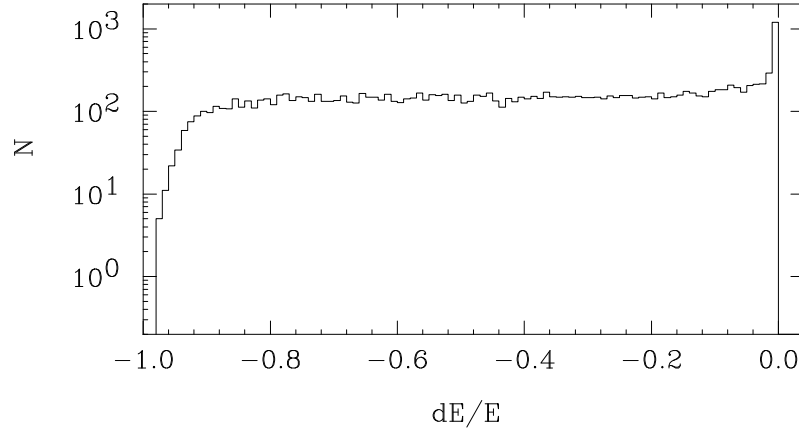


Figure 6: Energy distribution for the high disruption beam (15,000 particles).

by a factor of 3-4 compared to the nominal beam. This larger divergence translates into larger beam size in the quadrupoles, and therefore larger quadrupole apertures are required. Secondly, as seen in Fig. 2 and 6, the low energy tail in the high disruption beam is much more populated than in the nominal beam option. For comparison, the nominal disruption beam has about 1.2% low energy particles with δ below -60%, while the high disruption beam has 30% particles in this range and 10.6% particles with δ below -80%. To achieve beam loss in the high disruption case similar to the nominal case (about 5 kW), the chromatic bandwidth of the extraction line has to be increased to $\delta = -92\%$ from the -70% for the nominal beam. Thus, the lowest particle energy accepted by the optics has to be further reduced by a factor of 4. Note that at $\delta = -92\%$ the particles experience 12 times larger deflections in the magnets compared to the on-momentum beam. These very large deflections make it difficult to confine the tail particles within the aperture.

4 Study of High Disruption Beam Loss

As a first step, we verified the high disruption beam loss for the current extraction line design. In the simulations, we used disrupted beam distributions at the IP generated with GUINEA-PIG code [6], and then tracked the beam to the dump using modified DIMAD code which correctly simulates large energy deviations [8]. With 15,000 initial particles, the total beam loss was 28.2% particles, all in the range of δ below -60%. Most of these losses are due to the very low energy particles, but are also enhanced by the large beam divergence at the IP. About half of the beam loss (15.2%) occurred in the five-quadrupole system after IP.

Clearly, the above losses need to be significantly reduced for a realistic design with high disruption beams. Below we describe various methods we tried to reduce the beam loss. However, more studies are needed for an acceptable solution.

Finally, note that in this paper we discuss one particular option for the high disruption beam parameters (Table 2). There are other scenarios with less severely disrupted beams which still benefit from the near-equal beta functions at the IP [3]. There are also parameters for high luminosity operation at 1 TeV with ‘flat’ beams that have much smaller disruption and beamstrahlung [2].

4.1 Optics Modifications

As mentioned earlier, a large portion of the high disruption beam (15.2% particles) is lost in the five quadrupoles after IP. It indicates that the optics optimization has to begin with this quadrupole system. The main causes of the excessive beam loss are: much larger than nominal the low energy tail and increased beam divergence at the IP.

The larger IP divergence increases the beam size in the quadrupoles. To improve the quadrupole acceptance, we increased the quadrupole aperture by a factor of 2 (for instance, from $a_p = 10$ to 23 mm in the first quad, etc., where a_p is the pole tip radius). For realistic design, we kept the quadrupole pole tip field B_p below 12 kG. The resultant reduction in field gradient B_p/a_p was compensated by lengthening of the quadrupoles. The longer quadrupoles, in turn, increase the beam size; thus, both the length and aperture were optimized.

The quadrupole focusing depends on energy as $\frac{KL}{1+\delta}$, where KL is the on-momentum focusing strength. In the high disruption beam most losses are caused by the low energy over-focusing. This happens when the quadrupole off-momentum focal distance $\frac{1+\delta}{KL}$ becomes too small compared to the distance between quadrupoles. One way to reduce this effect is to make smaller the on-momentum KL values. This can be done by increasing the number of alternating gradient quadrupoles after IP. Since the total on-momentum focusing in the quadrupole system has to remain about the same (to focus to the secondary IP), the individual quadrupole KL values are reduced with more quads. As a result, the low energy particles experience less deflections in each quadrupole and less betatron amplitude in the system. The disadvantages of this method are the longer quadrupole system, the increased on-momentum beam size and larger aperture.

In this study, we added one more quadrupole to make a six-quadrupole system after IP. Due to the larger aperture and additional quadrupole, the length of this focusing system

increased from the current 25.2 m to 45.8 m. The quadrupole parameters were optimized to provide at least $5\sigma_x/10\sigma_y$ disrupted beam acceptance in the quadrupoles within the energy range of δ from 0 to -70%. The resultant apertures vary from $a_p = 23$ mm in the first quadrupole to 69 mm in the sixth quadrupole (compare to $a_p = 10$ to 32 mm in the current lattice).

The described lattice option for the high disruption beam is shown in Fig. 7. The parameters of the last quadruplet were also optimized for the maximum acceptance. The apertures of these quadrupoles range from $a_p = 114$ to 157 mm and were defined by the ± 1 mrad IP divergence of the beamstrahlung photon beam. In the chicane, the bend x/y -apertures were increased from $\pm 202/50$ mm to $\pm 250/108$ mm. For realistic design, the long quadrupoles were made of a number of short quadrupoles with gaps between them.

Tracking simulation with the high disruption beam showed that the total beam loss in the modified lattice is still very high: 21.2% particles versus 28.2% in the original lattice. Despite the larger quadrupole apertures after IP, about 14.7% particles are lost in the six-quad system. The energy distribution of the lost and survived particles is shown in Fig. 8. Clearly, all of the beam losses occur in the low energy tail at δ below -60%. The analysis of the beam distribution at IP showed that the highest energy lost particles ($\delta \approx -60\%$) had also large horizontal angles at IP, while the particles with small IP angles survived up to $\delta \approx -75\%$.

For comparison, we tracked the nominal disruption beam in this modified lattice. The total beam power loss reduced to 3.9 kW (4.8 kW in the original lattice), and the number of lost particles reduced from 0.25% to 0.23%. The power loss distribution in the modified lattice is shown in Fig. 9 and the energy distribution of the lost and survived particles is shown in Fig. 10. Note that increased bandwidth in Fig. 10 compared to Fig. 8 is due to smaller IP angular divergence in the nominal disruption beam.

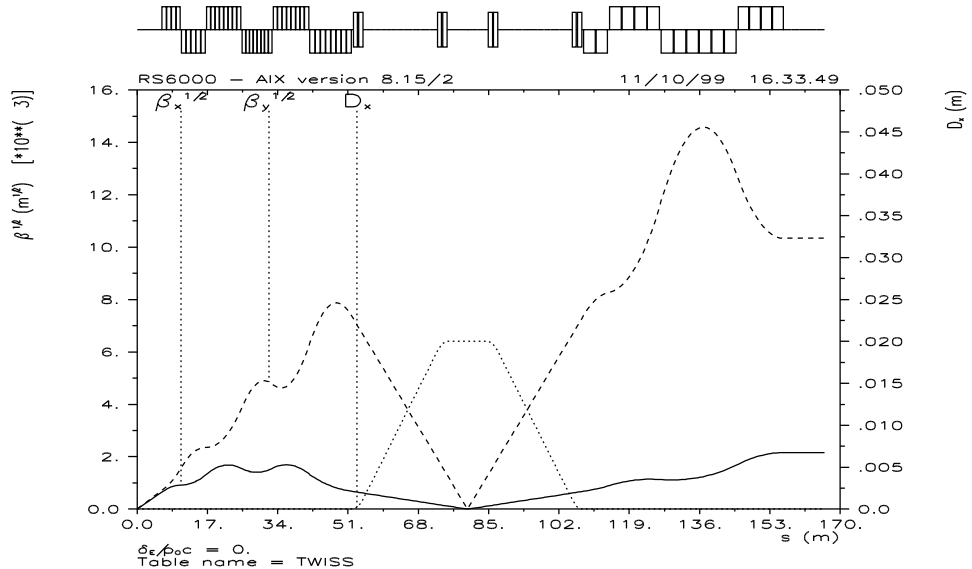


Figure 7: Lattice option for the high disruption beam.

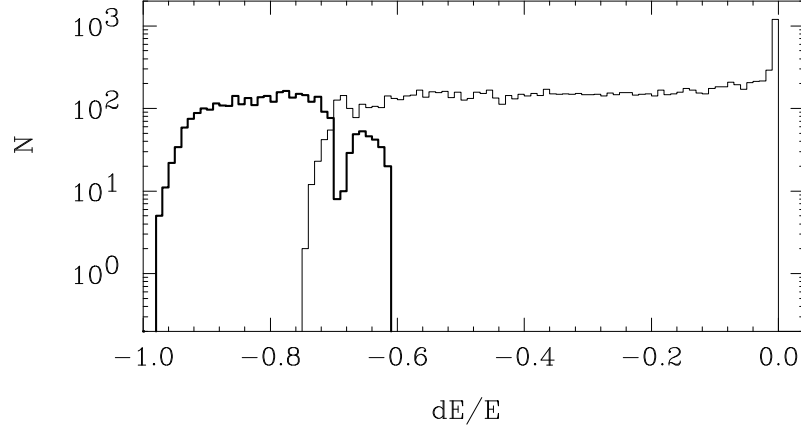


Figure 8: Energy distribution for the lost (thick line) and survived (thin) high disruption beam particles in the modified lattice (15,000 particles).

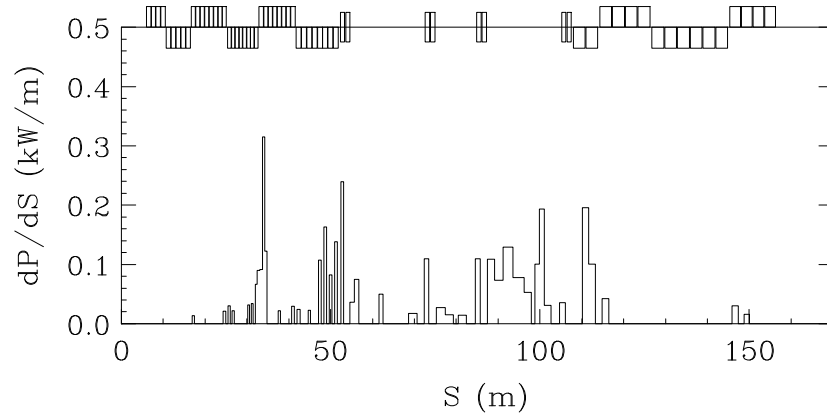


Figure 9: Power loss distribution for the nominal disruption beam in the modified lattice (NLC 1 TeV case A).

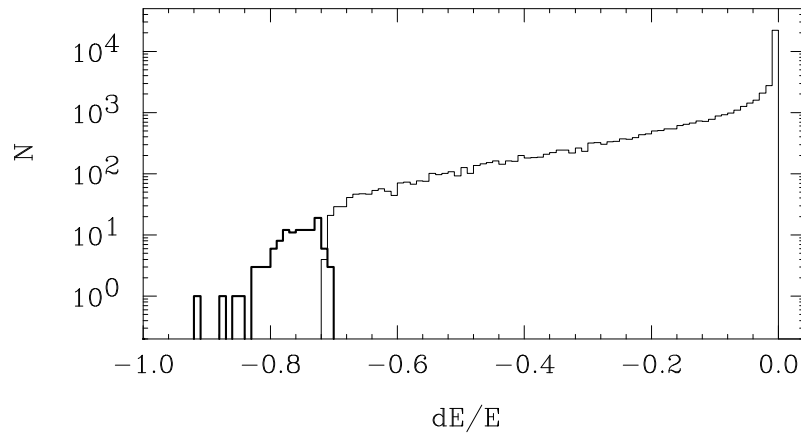


Figure 10: Energy distribution for the lost (thick line) and survived (thin) nominal disruption beam particles in the modified lattice (NLC 1 TeV case A; 50,000 particles).

Since the particle deflections in the quadrupoles increase at low energies rather fast ($\sim 1/\text{energy}$), very large magnets would be needed for a significant improvement of the chromatic acceptance with the high disruption beam. Further discussions are needed to decide if the use of larger magnets is acceptable.

4.2 Sextupole Correction

In accelerators sextupoles are typically used to compensate linear and some high order deviations in quadrupole focusing caused by energy errors. The correction requires non-zero dispersion at the sextupoles to generate compensating quadrupole effect on the orbit of the off-momentum particles. For a small energy spread, the focusing in quadrupoles and sextupoles depends linearly on δ , therefore the correction works for all particles in the bunch. In the case of the high disruption beam with a very broad energy spread, the focusing and trajectories change non-linearly at large $|\delta|$ and the sextupole effect may vary significantly for particles with different energies.

To study the effect of sextupoles on high disruption beam loss, we added a sextupole to each of the first six quadrupoles in the modified extraction line lattice and a horizontal bend at $s = 2$ m from IP (4 m before the first quad) to generate dispersion. For the maximum effect, we assumed that the sextupole field can be superimposed over full length of the quadrupoles. Though a large dispersion helps reduce the sextupole field, its amplitude is limited by the quadrupole aperture a_p and desired energy acceptance. In our case, the bend at $s = 2$ m generates spread in off-momentum particle trajectories, so at the entrance of the first quadrupole the horizontal orbit as a function of energy is $x(\delta) = \eta \frac{\delta}{1+\delta}$, where η is the linear dispersion at this point. Applying $|x(\delta)| < a_p$ for $a_p = 23$ mm and $\delta > -92\%$ results in the maximum dispersion value of $|\eta| = 2$ mm. This corresponds to 8.34 kG·m field in the dispersion generating bend at 500 GeV.

Optimization of the sextupole strengths showed that this correction does not significantly improve the low energy beam acceptance. With the sextupole field effectively imposed over quadrupole length and for the optimized values of the pole tip field in the six sextupoles ($B_p^{sext} = 4, 0.5, -9.5, 13, -5, -1$ kG), the particle loss at the end of the six-quadrupole system is reduced from 14.7% to 11.3%. This marginal reduction in the beam loss seems to not justify the complications of an extra bend near IP, superimposed sextupole and quadrupole fields and the need for dispersion cancellation after the sextupoles.

4.3 Octupole Correction

In a separate study, we investigated the effect of octupoles on the beam loss. As in the case with sextupoles, we effectively superimposed six octupoles over the six quadrupoles after IP. Since the octupole field increases as a cube of a particle amplitude, we consider that its most effect will be on the low energy particles experiencing large deflections in the quads, and will not significantly affect the rest of the beam.

In quadrupoles the beam is focused or defocused either in horizontal or vertical direction. Accordingly, the main losses of the low energy particles are expected to be in x and y -planes

(see Fig. 5). Octupoles also provide horizontal and vertical focusing which can be used to compensate the quadrupole effect at large amplitudes. Compared to the quadrupoles, a normal octupole provides simultaneous non-linear focusing along the x and y -axes and defocusing along the $|x| = |y|$ lines, or vice versa.

In the quadrupole system the net x and y focusing is dominated by the horizontally (F) and vertically (D) focusing quads, respectively. Therefore, to reduce the net low energy over-focusing in both planes one has to reduce the horizontal focusing in F-quads and vertical focusing in D-quads. Since the octupoles simultaneously focus (or defocus) in the x and y -planes, all six compensating octupoles need to be defocusing in order to reduce the quadrupole focusing at large amplitudes.

In simulations, we varied the individual octupole strengths and confirmed that the six octupoles have to be defocusing for the most reduction of the high disruption beam loss. The same aperture and effective length was used for the combined octupoles and quadrupoles. Fig. 11 shows the particle loss as a function of octupole pole tip field (same for the six octupoles). For realistic field values the particle loss at the end of the six-quadrupole system reduces to 12.6% from 14.7% without octupoles. This is rather small improvement and we do not yet consider this compensation as a practical solution.

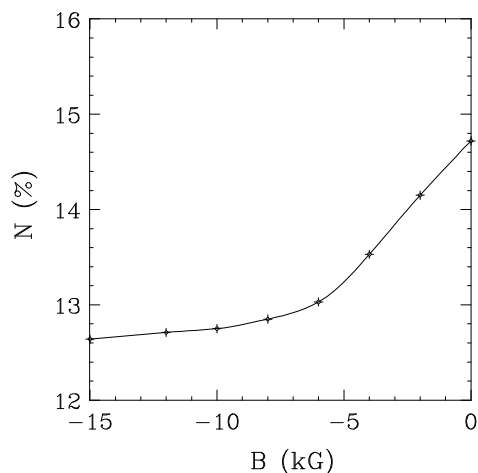


Figure 11: High disruption beam loss $N(\%)$ at the end of the six-quadrupole system versus octupole pole tip field.

4.4 Low Energy Tail Separation

An alternative way to avoid large beam loss in the extraction line is to separate the low energy tail from the beam and direct it to a different transport line. In this case, the energy acceptance requirement can be relaxed for the main beam extraction line and the transport line for the tail can be better adjusted for the lower energy or designed to absorb the energy. Since the large losses start in the quadrupoles after IP, the separation has to be done before the beam enters the quads.

Dipole bending naturally spreads the particle trajectories with different energies. The low energy particles experience the largest deviations from the on-momentum orbit, which are proportional to $\frac{\delta}{1+\delta}$. For the beam separation study, we introduced a symmetric horizontal chicane between $s = 6$ and 18.6 m after IP and moved the first quadrupole to $s = 18.9$ m as shown in Fig. 12. Each individual chicane bend is 1.2 m long and has 12 kG field at 500 GeV. The goal for the first two chicane bends was to generate a large spread between trajectories of the low energy particles and the core beam. Then the septum bends in the middle of chicane are used to deflect back only the core beam particles and allow the low energy tail travel unbent into a different transport line. The dispersion at the end of the chicane is canceled, and if the energy spread in the beam is significantly reduced after the tail separation, then a simpler quadrupole system, such as a doublet, can be used to focus to the secondary IP.

We used the beam separation condition which required that the separated tail particles did not strike the face of the first quadrupole located at $s = 18.9$ m. In other words, the septum bends would separate only the tail particles with deflection at the first quadrupole larger than the outer quadrupole radius. We estimated that the aperture of the first quadrupole needs to be about $a_p \approx 60$ mm and the outer radius of such a permanent magnet with 12 kG pole tip field can be on the order of 150 mm.

The high disruption beam distribution was tracked through the first two deflecting bends, and Fig. 13 shows the horizontal angular divergence versus energy at the entrance to the first separating septum bend at $s = 9.6$ m. The horizontal phase space at this point is shown in Fig. 14, where the vertical line at $x = -34.8$ mm separates the beam core and the tail. Counting the particles shows that only 3.1% particles are in the tail. The energy distributions of the core and tail beams are shown in Fig. 15.

Since the number of low energy particles in the core beam is still large after the separation, we conclude that the above scheme is not very effective. For this reason we did not proceed to study other important issues such as the design and efficiency of septum bends and the transport line for the low energy tail.

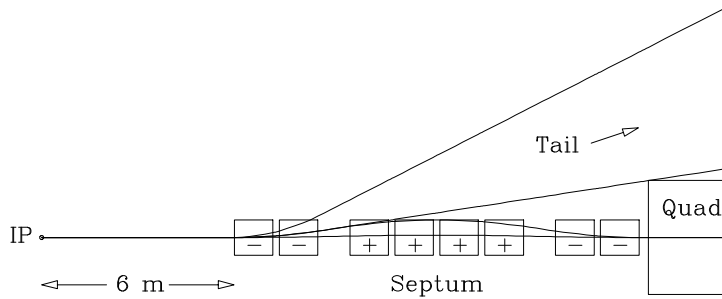


Figure 12: Beam separation with chicane and septum bends.

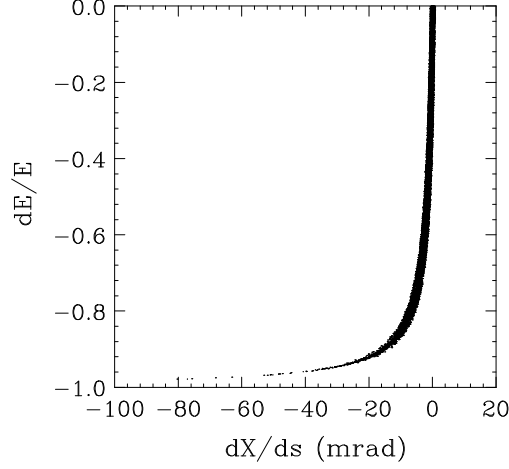


Figure 13: Horizontal angular distribution vs. energy at the separating septum bend.

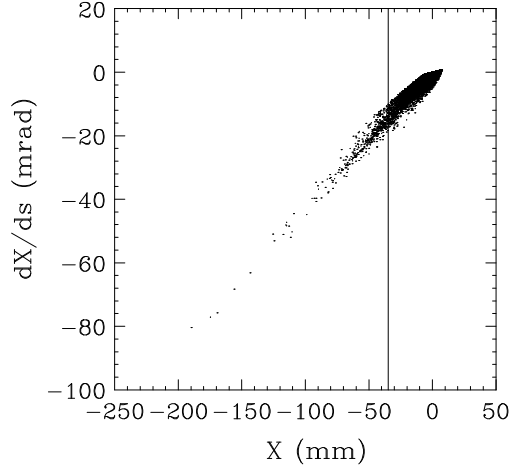


Figure 14: Horizontal phase space distribution of the high disruption beam at the separating septum bend. The vertical line separates the tail (on the left) from the core.

5 Summary

We investigated various methods to reduce the beam loss in the NLC extraction line caused by a large number of very low energy particles in the high disruption beam option. The study included the use of larger quadrupole aperture, weaker quadrupole focusing, sextupole compensation, octupole focusing at large amplitudes, and beam tail separation with chicane septum bends. We did not find significant reduction of the beam loss with the above methods. Further studies and new ideas are needed to find a practical solution for the high disruption scenario.

References

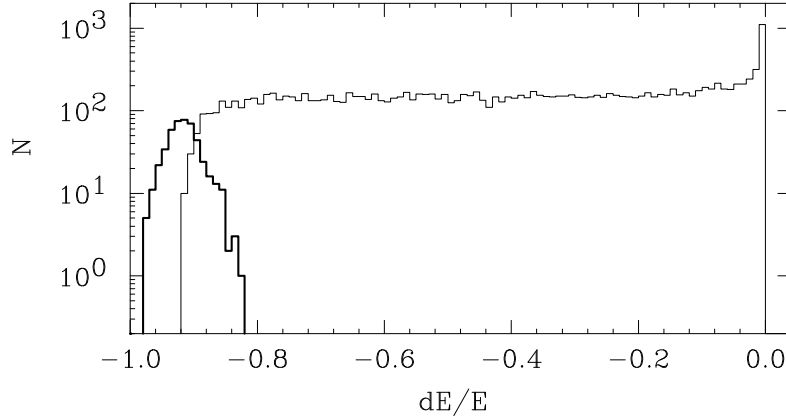


Figure 15: Energy distribution for the tail (thick line) and the core (thin) high disruption beams at the separating septum bend (15,000 particles).

- [1] K. A. Thompson and T. O. Raubenheimer, “Luminosity for NLC Design Variations,” SLAC note LCC-0014 (1999); on the web at:
http://www-project.slac.stanford.edu/lc/ilc/TechNotes/LCCNotes/lcc_notes_index.htm.
- [2] T.O. Raubenheimer, “Parameters and Possible Operating Modes of the NLC,” SLAC note LCC-0031 (1999); on the web at:
http://www-project.slac.stanford.edu/lc/ilc/TechNotes/LCCNotes/lcc_notes_index.htm.
- [3] K. A. Thompson, *et al.*, “High-luminosity NLC Designs with Near-equal Horizontal and Vertical Beta Functions,” SLAC note LCC-0022 (1999); on the web at:
http://www-project.slac.stanford.edu/lc/ilc/TechNotes/LCCNotes/lcc_notes_index.htm.
- [4] Y. Nosochkov, *et al.*, “The Next Linear Collider Extraction Line Design,” Proceedings of the 1999 IEEE Part. Acc. Conf. (PAC99), New York City, NY (1999); SLAC-PUB-8096 (1999).
- [5] M. Woods [SLD Collaboration], “The Scanning Compton Polarimeter for the SLD Experiment,” Proceedings of the 12th International Symposium on High-Energy Spin Physics (SPIN 96), Amsterdam, Netherlands (1996); SLAC-PUB-7319 (1996).
- [6] The disrupted beam distributions were calculated by K. A. Thompson using GUINEA-PIG code [7].
- [7] D. Schulte, Ph.D. thesis (1996).
- [8] P. Tenenbaum, *et al.*, “Use of Simulation Programs for the Modeling of the Next Linear Collider,” Proceedings of the 1999 IEEE Part. Acc. Conf. (PAC99), New York City, NY (1999); SLAC-PUB-8136 (1999).